A van der Waals Density Functional Investigation on the Improved Adsorption Properties of NO on the Rh$_n$/MgO (100) Interface

Guoli Zhou,[†] Pan Li,[†] Zhixue Tian,[*,†] and Ying Liu[†,‡]

[†]Department of Physics and Hebei Advanced Thin Film Laboratory, Hebei Normal University, Shijiazhuang, Hebei 050024, China
[‡]State Key Lab of Nonferrous Metals & Processes, General Research Institute for Nonferrous Metals, Beijing 100088, China

ABSTRACT: Using spin-polarized density functional theory calculations, we have studied the interaction and morphology of small Rh$_n$ clusters ($n \leq 5$) deposited on a MgO (100) surface, as well as the ability of Rh$_n$/MgO systems to trap NO molecules. We show that Rh$_n$ clusters can tightly adhere to a MgO (100) surface because of hybridization of O 2p and Rh 4d orbitals. The most energetically preferred structure for each adsorbed Rh$_n$ cluster looks similar to the structure of the isolated cluster, except for an increment in the length of base edge(s) close to the substrate. We find that the Rh$_n$/MgO system exhibits a much stronger ability to trap NO, especially for Rh$_2$ and Rh$_4$ clusters, than do the bare Rh$_n$ clusters. The hybridization of N 2p and Rh 4d orbitals is responsible for the strong adsorption of NO on Rh$_n$/MgO. This can be explained by the increased Rh−Rh bond length that results in a decrease in the effective coordination number, and the presence of extra electrons obtained from the substrate, causing the N and O atoms to bond strongly to the Rh atoms, which in turn weakens the N−O molecular interaction. Additionally, binding to NO induces a reduction in the total magnetic moment of the Rh$_n$/MgO system. Thus, putting Rh$_n$ on the MgO (100) surface can decrease competition between bonding and magnetism. However, whether it can be related to improve trapping of NO deserves further investigations.

KEYWORDS: adsorption, interface, van der Waals density functional, cluster, magnetism
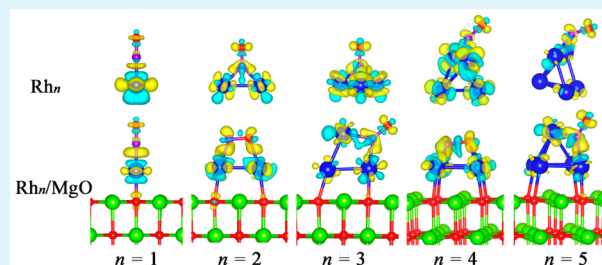
I. INTRODUCTION

The precious metals Rh, Pd, and Pt are known in the chemical industry to be excellent catalysts. For instance, they are widely used in three-way catalysts to convert the toxic exhaust emissions from motor vehicles into harmless gases. In this context, Rh has been considered to be the most efficient catalyst for facilitating the dissociation of the N−O bond.[1] The crucial step in this process is the dissociation of NO on the catalyst. However, because of the shortage of precious metals, how to retain the high activity of Rh and also reduce the consumption of this precious metal has become a challenge. Therefore, exploring approaches to improve the activities of small precious metal particles is of great significance.

The study of small metal clusters has greatly expanded due to interest in their nanostructures and their unique electronic,[2] magnetic,[3] and catalytic properties.[4−10] As compared to Rh surfaces, the Rh$_n$ clusters exhibit superiority in trapping NO. The calculated magnitudes of NO binding energies on Rh$_n$ clusters (-3.23 to -2.77 eV)[11] are larger than those on Rh (100) (-2.59 eV) and (111) (-2.18 eV) surfaces.[12] In addition, unlike nonmagnetic bulk Rh, the Rh$_n$ clusters also exhibit remarkable magnetism, as was first proposed by Reddy et al.[13] on the basis of their DFT calculations and subsequently confirmed experimentally.[3,14] In particular, experimental investigations have shown that bare Rh clusters have very large magnetic moments, decreasing with the size of the cluster. Recently, much effort has been devoted to studying the

structure, binding energies, and magnetic properties of Rh clusters using DFT.[15−18] One earlier DFT study on the interaction of NO with Rh$_2$[19] found that the N−O bond length was increased as compared to its gas phase value. In addition, a series of theoretical and experimental studies[6,7,20] has systematically examined the behavior of NO on Rh$_6^+$ clusters. They have shown that the dissociation of NO has a rather lower energy barrier than it does on the Rh (100) surface. Recently, Ghosh et al.[11] have carried out first-principles calculations to study the binding of NO to small Rh clusters (from Rh$_1$ to Rh$_5$) with and without spin-polarization as a function of the effective coordination number (or the cluster size). The binding energy of NO was found not to change significantly with the cluster size and the effective coordination number, being attributable to the dramatic magnetic quenching of the Rh clusters upon adsorbing NO, which thus competes with binding. This is unlike the results obtained in their later work.[21] In subsequent work (Pushpa et al.[21]), they investigated the changes in the adsorption and dissociation of NO on a series of Rh surfaces, including unstrained and strained Rh (100) surfaces and monolayers of Rh atoms on strained and unstrained MgO (100) surfaces. They found that as the effective coordination number decreases, the d-band center of the Rh atoms shifts

Table 1. Structure, Cohesion Energy (CE = $[E(Rh_n) - nE(Rh)]/n$), and Magnetic Moment (M) Calculated Using the vdW-DF and PBE Functionals for the Rh_n ($n = 2-5$) Clusters in the Gas Phase[e]

n	structure	d (Rh-Rh) (Å)	CE (eV/atom)	M (μ_B)
2		$2.21^{v,p}$ (2.22^a, 2.26^b,2.28^c)	-1.92^v, -1.62^p (-2.02^a)	$4.0^{v,p}$ ($4.0^{a,d}$)
3		2.37^v, 2.40^p (2.39^a, 2.42^b)	-2.57^v, -2.23^p (-2.63^a)	$3.0^{v,p}$ ($3.0^{a,d}$)
4		2.44^v, $2.42/2.78^p$ (2.45^a, 2.49^b)	-3.05^v, -2.64^p (-3.11^a)	0.0^v, 6.0^p ($0.0^{a,d}$)
5		$2.39/2.56^v$, $2.40/2.57^p$ ($2.40/2.56^a$, $2.48/2.63^c$)	-3.34^v, -2.93^p (-3.38^a)	5.0 ($5.0^{a,d}$)

[a]Reference 39. [b]Reference 40. [c]Reference 41. [d]Reference 42. [e]The superscripts "v" and "p" indicate results obtained using the vdW-DF and PBE functionals, respectively.

closer to the Fermi level, and the NO molecule adsorption as well as N and O coadsorption become stronger. As discussed by Pushpa et al., approaches to reduce the effective coordination number may also tend to produce magnetism that resists the bonding. Thus, it is suggested that in ensuring a sufficiently small effective coordination, one should ensure that the negative effects of the magnetism are not too evident.

Clusters of precious metals placed on oxide surfaces have been found to improve the catalytic activities of the oxides. For instance, doping Pt_4 clusters onto the (100) surface of $La_{0.625}Sr_{0.375}Co_{0.25}Fe_{0.75}O_{3-\delta}$ can greatly enhance the adsorption and dissociation of O_2.[22] Theoretical investigations have shown that Pt-loaded anatase TiO_2 has a higher catalytic activity for the conversion of nitrobenzene than do pure Pt clusters.[23] Such an improvement is attributed to a strong interaction between the precious-metal clusters and the oxide surfaces. Thus, in the present work, we have performed spin-polarized DFT calculations on the binding effect of NO to small Rh_n clusters ($n \leq 5$) deposited on a free MgO (100) surface. The selection of the MgO {100} surface as the substrate was based on its very simple atomic structure, the strong ionic bonding characteristics, excellent thermal and chemical stability, and its unreconstructed surface with little rumpling.[24−26] The main motivation of our work is to study the variations in the structures and magnetism of Rh_n clusters deposited on the MgO (100) surface, and to compare the binding effects of NO on bare Rh_n clusters and in the Rh_n/MgO systems.

As was the case in ref 27, to obtain the correct interfacial properties, the cohesion energies and bond lengths of the Rh_n clusters on MgO (100) surfaces were calculated using three distinct functionals: the conventional GGA and LDA functionals, and the recently developed nonlocal vdW-DF functional. Subsequent results, particularly those for the bonding of NO, were calculated using only the vdW-DF functional. The remainder of this Article is organized as follows: In section II, we present some of the technical details of our computational method. In section III, we show and discuss our results concerning the structure of Rh_n clusters on MgO and the interactions between them, and compare the binding strength of NO to the bare Rh_n clusters and to Rh_n clusters on MgO. Finally, we summarize our results in section IV.

II. COMPUTATIONAL METHOD

First-principles DFT calculations were performed using the Vienna ab initio simulation package (VASP).[28−30] The projector augmented wave (PAW) method was adopted to deal with the electron−ion interactions.[31,32] The cutoff energy for the plane wave basis set was fixed at 400 eV. Spin-polarization was employed for all calculations except where specifically noted. For comparison purposes, we used three exchange-correlation functionals, the LDA,[33] GGA in PBE[34] form, and the vdW-DF[35] to calculate the adhesion properties of Rh_n clusters to MgO (100) surfaces. For the binding of NO to Rh_n clusters with and without the MgO surface, only vdW-DF was used. The vdW density functionals are implemented in the VASP code with the efficient algorithm of Román-Pérez and Soler.[36,37]

The MgO (100) surface was constructed using four MgO slabs. To avoid lateral interactions between the periodic Rh clusters, we used a p (4 × 4) unit cell in the xy-2-dimensional plane for the substrate, containing 128 atoms. A (3 × 3 × 1) Monkhorst−Pack k-point mesh[38] was used for all of the Rh_n/MgO (100) interfaces with and without binding of NO. To simplify comparison, we also calculated the binding of NO on free Rh_n clusters, using only the Γ point. All atoms were allowed to fully relax. The energy relaxation was continued until the forces on all of the atoms had converged to less than 0.02 eV/Å.

The adhesion energy, E_{adh}, of Rh_n clusters on the MgO (100) surface was defined as

$$E_{adh} = E(Rh_n/MgO) - E(Rh_n) - E(MgO) \tag{1}$$

in which $E(Rh_n/MgO)$, $E(Rh_n)$, and $E(MgO)$ are the total energies of the Rh_n/MgO systems, the relaxed isolated Rh_n cluster, and the bare MgO surface as a substrate.

The binding energies, E_{ads}, of NO on the Rh_n cluster with and without the MgO (100) surface were defined as

$$E_{ads} = E(NO-Rh_n/MgO) - E(NO) - E(Rh_n/MgO) \tag{2}$$

$$E_{ads} = E(NO-Rh_n) - E(NO) - E(Rh_n) \tag{3}$$

where the three items on the right-hand side of each expression represent the total energies of the NO−Rh_n/MgO complex, the NO molecule in the gas phase, and the Rh_n cluster with and without the MgO substrate.

III. RESULTS AND DISCUSSION

1. Small Rh_n ($n = 1-5$) Clusters on MgO (100) Surface. We first present in Table 1, the properties, that is, geometries, energies, and the total magnetic moments, of small Rh_n clusters, to provide a basis for understanding the growth behavior of Rh_n clusters on the MgO (100) surface. We have examined all of
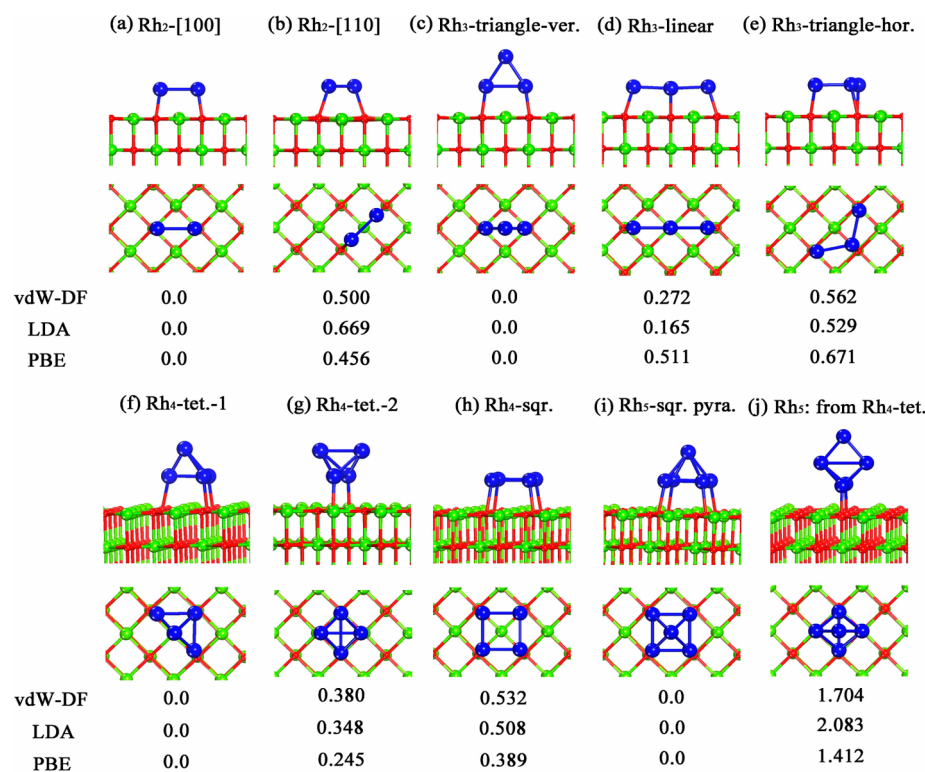
	(a) Rh₂-[100]	(b) Rh₂-[110]	(c) Rh₃-triangle-ver.	(d) Rh₃-linear	(e) Rh₃-triangle-hor.
vdW-DF	0.0	0.500	0.0	0.272	0.562
LDA	0.0	0.669	0.0	0.165	0.529
PBE	0.0	0.456	0.0	0.511	0.671

	(f) Rh₄-tet.-1	(g) Rh₄-tet.-2	(h) Rh₄-sqr.	(i) Rh₅-sqr. pyra.	(j) Rh₅: from Rh₄-tet.
vdW-DF	0.0	0.380	0.532	0.0	1.704
LDA	0.0	0.348	0.508	0.0	2.083
PBE	0.0	0.245	0.389	0.0	1.412

Figure 1. Side (up) and top (down) views for the energetically preferred Rh_n/MgO (100) structures. Panels (a) and (b) are for Rh_2/MgO, (c)−(e) present the Rh_3/MgO interfaces, (f)−(h) show the three Rh_4/MgO interfaces, and (i) and (j) are for the Rh_5/MgO structures. The blue, green, and red balls represent Rh, Mg, and O atoms, respectively. The total energy differences (in eV) with respect to the most stable state are shown below each diagram for the three different functionals, vdW-DF, LDA, and PBE.

the possible structures of isolated Rh_n clusters using the three functionals mentioned above. Only the most energetically preferred geometries obtained from the vdW-DF and PBE calculations are presented in Table 1. The two functionals predict the same optimized structures for the Rh_n clusters, except for Rh_4. To ease comparisons, Table 1 also includes results calculated in other theoretical studies. It may be seen that our results from the vdW-DF calculations are quite consistent with the previous calculations,[39−43] but the PBE functional slightly underestimates the cohesion energy of the clusters. For a Rh dimer, the cohesive energy is about 1.92 eV, which is slightly weaker than that given in ref 36. The bond length of 2.21 Å is close to the experimental value. The total magnetic moment (TMM) of the dimer is 4 μ_B, also in agreement with earlier work.[42,43] The most stable structure of the trimer is an equilateral triangle, with a bond length of 2.37 Å and a magnetic moment of 3 μ_B. For the isomers of Rh_4, a nonmagnetic tetrahedron with a bond length of about 2.44 Å is predicted to be the lowest-energy configuration by the vdW-DF functional. However, a tetrahedron with a magnetic moment of 6 μ_B and a square geometry with a magnetic moment of 4 μ_B also exist. These isomers are less stable than the nonmagnetic tetrahedron, but only by about 0.025 and 0.05 eV/atom, respectively. We have also used the DMol3[44] and the Quantum Espresso codes[45] to verify the stability and magnetism of tetrahedral Rh_4, and obtained the same results. However, the PBE functional predicts that the tetrahedron with a magnetic moment of 6 μ_B is slightly more stable than the others. We note that our vdW-DF results are consistent with some previous studies,[13,39,40] and PBE gives the same result as that presented in ref 11. As in previous studies, the square pyramid, with a

magnetic moment of 5 μ_B, is calculated to be the lowest-energy configuration for Rh_5. We note that as the cluster size increases, the magnitude of the cohesive energy of the clusters increases because of the increased atomic coordination.

We next put the Rh_n clusters onto the MgO (100) surface. The adsorption site of a single Rh atom was examined by placing it on three possible sites: (i) on top of a Mg atom, (ii) on top of an O atom, and (iii) above the 4-fold hollow site between Mg and O atoms. Similarly to the case for silver,[27] Rh tends to occupy the on-top-of-O site, with a binding energy of −2.117 eV. For the Rh_n clusters with $n > 1$, the Rh atoms were set to reside at the same adsorption sites mentioned above with various possible geometries. The two or three most stable structural isomers obtained from energy minimization are shown in Figure 1. It was found that the three functionals identified the same structures as being most stable for each Rh_n cluster on the MgO surface. For the Rh dimer, the two Rh atoms prefer to align on the O sites in the {100} direction. The distance between the two Rh atoms was found to be 2.48 Å, about 0.27 Å larger than that for an isolated dimer. For the adsorption of Rh_3, the most stable geometry found was an isosceles triangle with two Rh atoms bonded to the substrate and one standing away from the substrate. The bottom Rh−Rh bond adjacent to the MgO surface was enlarged to 2.53 Å, and the other two bonds contracted but only by 0.02 Å. The most stable linear Rh_3 isomer was 0.27 eV higher in energy than the triangular state. From Figure 1f−h, three Rh_4 geometries are seen to be relatively stable on the MgO surface, two tetrahedrons and one square. The tetrahedral-Rh_4 cluster with three Rh atoms bonding to the substrate (Figure 1f) is the most stable state on the MgO surface, with an energy 0.380 and

0.532 eV lower than the other tetrahedron with only two Rh atoms bonded to the MgO surface (Figure 1g) and the square (Figure 1h). The same structure was also found for Ir$_4$ deposited on a MgO (100) surface.[46] In the case of the two tetrahedrons, the bond lengths of the two vertical Rh–Rh bonds in different planes were increased to 3.35 and 2.70 Å (near the substrate) and 2.55 and 2.65 Å (exposed to the vacuum), respectively, and the others remained almost unchanged. The four Rh–Rh bonds in the square all have the same bond length. For Rh$_5$, we examined two initial geometries on the MgO (100) surface. One was the Rh$_5$ ground state for the isolated cluster, the square pyramid, and the other was defined by adding an additional Rh atom to the optimized tetrahedral Rh$_4$ cluster. It turned out that the square pyramid had a much stronger binding to the MgO surface than the latter, with the energy difference being as large as 1.70 eV. The bond lengths of the Rh–Rh bonds in the bottom square were 2.44 Å, increased by 0.05 Å in comparison to those of Rh$_5$ in vacuum. In general, it may be seen in Figure 1 that the base bond(s) of the Rh$_n$ clusters adjacent to the MgO surface are significantly enlarged, while the other Rh–Rh bonds show almost no changes in comparison to the isolated clusters, indicating the effect of the smaller effective coordination number.[11]

The calculated adhesion energies of the Rh$_n$ clusters to the MgO surface calculated using the three exchange-correlation functionals are presented in Figure 2. From Figure 2, the three
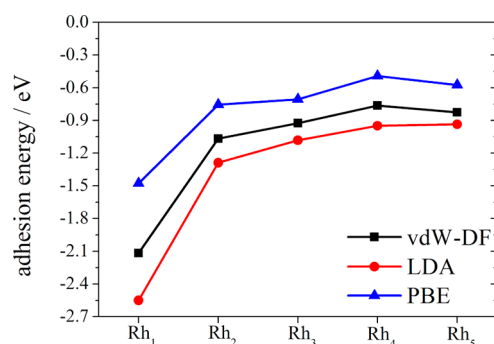

Figure 2. Calculated adhesion energies (E_{adh}, in eV) of the Rh$_n$ clusters to the MgO (100) surface as a function of the cluster size obtained using the vdW-DF, LDA, and PBE functionals.

functionals may be seen to predict a similar trend for the adhesion energies. As expected, the PBE and LDA functionals yield the weakest and strongest adhesions, respectively, and the

vdW-DF result lies in between. Because the same morphologies were obtained using all three functionals and because the adhesion energies obtained from the vdW-DF calculations were intermediate to the values obtained using the PBE and LDA functionals, further discussions and calculations for NO bonding to the Rh$_n$/MgO systems are all for the results obtained using the vdW-DF functional.

It may be seen from Figure 2 that the isolated Rh atom has the strongest adhesion on the MgO surface. Bader topological analysis shows that the single Rh atom gains 0.33 electrons from the MgO surface. From the charge density difference shown in Figure 3b, we find that the additional electrons occupy the Rh $4d_{xy}$ orbital. In the case of Rh$_n$ with $n \geq 2$, the adhesion decreases due to the metal–metal lateral interaction becoming dominant. On the basis of Bader analysis, the average number of electrons transferred from the substrate to each Rh atom of Rh$_n$ ($n = 2, 3, 4, 5$) clusters is 0.30, 0.16, 0.16, and 0.15 e, respectively. Figure 3c–f indicates that the charge accumulations appear mainly in a plane lying horizontally with respect to the MgO surface and around the Rh atoms at the interface, leading to strengthening of the Rh–Rh interaction in the vicinity of the MgO surface. Figure 3a shows the corresponding planar averaged charge density difference for the Rh$_n$/MgO interfaces as a function of position in the z-direction. The charge redistribution occurs at the interface between the cluster and the MgO surface, which is highlighted by a yellow rectangle. The positive values denote electron accumulation, and the negative values indicate electron depletion. This further confirms that electrons transfer from the MgO surface to the Rh$_n$ clusters.

The charge redistribution is also accompanied by a change of the spin state for the Rh$_n$ clusters. In Table 2, we present the

Table 2. Total Magnetic Moments (in μ_B) of Rh$_n$ Clusters under Different Conditions: Bare Rh$_n$ with and without a MgO (100) Surface, Bonding to NO with and without a MgO (100) Surface ($n = 1$–5)

n	Rh$_n$	NO–Rh$_n$	Rh$_n$/MgO	NO–Rh$_n$/MgO
1	1.92	0.0	1.00	0.00
2	4.0	1.0	1.88	0.95
3	3.0	0.0	2.87	1.89
4-tet.-1	0.0	5.0	2.02	1.00
4-square	4.0	3.0	5.85	1.07
5	5.0	4.0	4.94	4.00

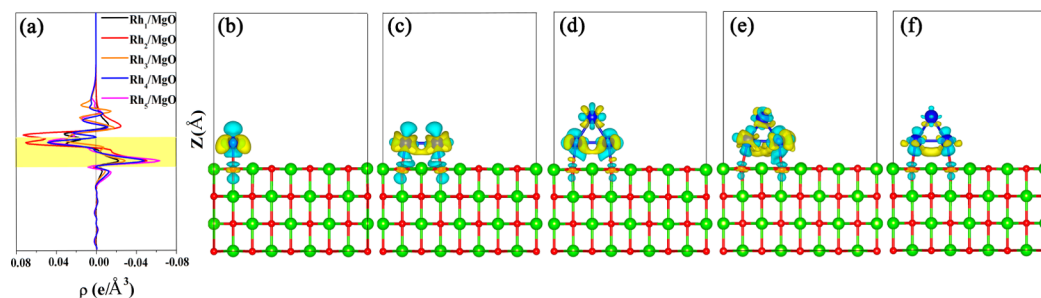**Figure 3.** Charge density differences ($\Delta\rho = \rho(Rh_n/MgO) - \rho(MgO) - \rho(Rh_n)$) for the Rh$_n$/MgO (100) interfaces are shown in panels (b)–(f). The yellow and blue regions indicate charge accumulation and depletion, respectively. The isosurface value is 0.005 e/Å^3. The corresponding planar averaged charge density differences for the five interfaces are plotted (in panel (a)) with different colored lines, as a function of position in the z-direction. The highlighted part represents the location of the interface.
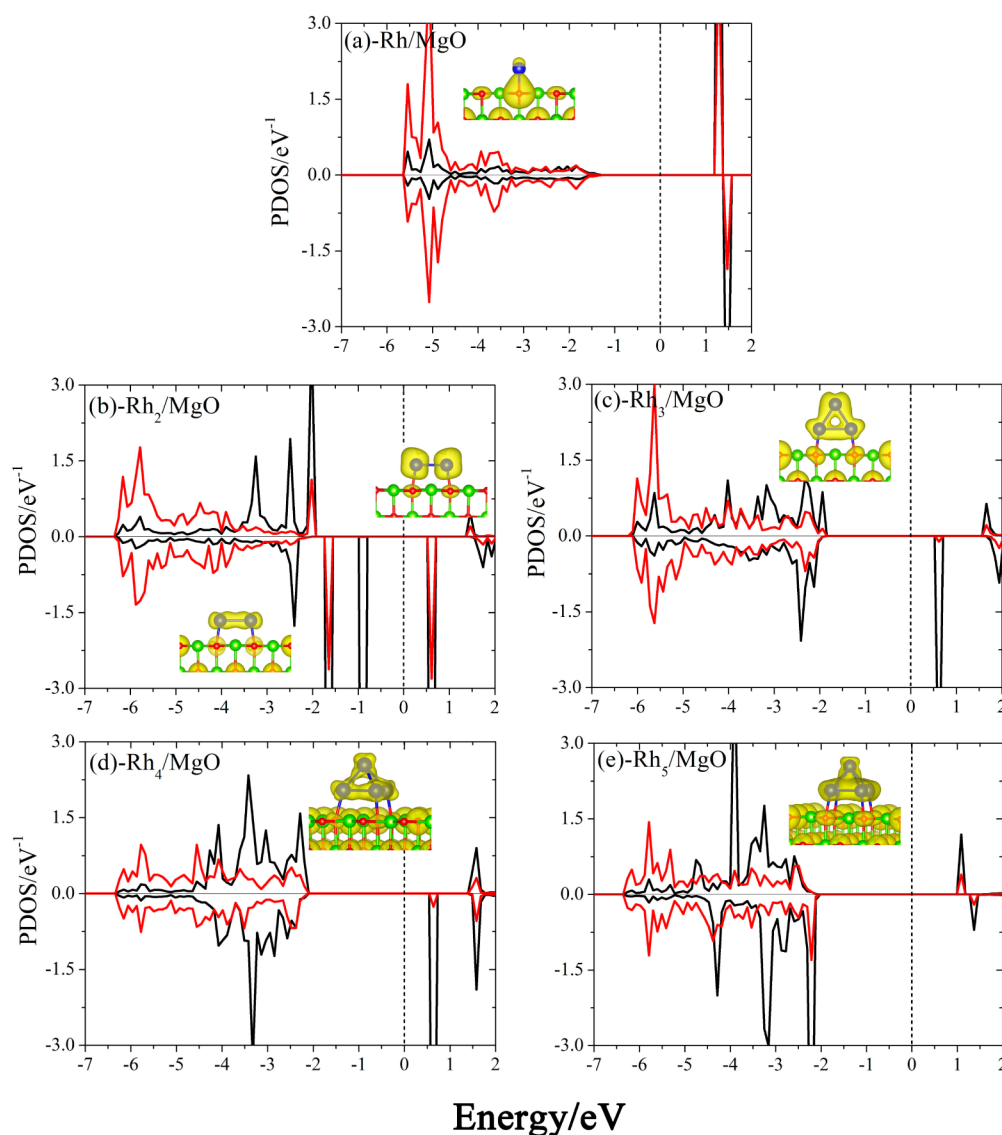
Figure 4. Projected DOS (PDOS) plotted in (a)−(e) are for the O atom and the closest-lying Rh atom in the Rh$_n$ cluster on the MgO surface. The red and black lines represent the O 2p and Rh 4d states, respectively. The Fermi level is set to zero energy. The partial charge densities in each panel correspond to the hybridizations of O−Rh and Rh−Rh bonds in the energy windows shown. Because of the similar interactions between O and Rh at low energy levels, the partial charge density of the Rh$_1$/MgO interface is also presented for comparison.

TMMs of the Rh$_n$ clusters in various systems. On the MgO (100) surface, the TMMs of single-atom Rh and of Rh$_2$ dimers decrease by one-half, due to the strong interfacial interaction. We can see in Figure 1f that the adsorption of the Rh$_4$ cluster increases the length of one Rh−Rh bond by almost 1.0 Å near the MgO surface. That is, it essentially cleaves one of the Rh−Rh bonds of the isolated cluster, resulting in an increased TMM of 2.0 μ_B. This strengthens the cluster interaction with the support. However, the TMMs of Rh$_3$ and Rh$_5$ remain unchanged because the length of the Rh−Rh bonds increases only slightly.

In Figure 4, we show projected DOS (PDOS) for Rh and its nearest neighbor O atom to gain more insights into the interactions and how they are affected by the presence of the MgO surface. For all five cluster sizes, the Rh-4d orbital loses electrons, but this is balanced by a significant hybridization between O p_z and Rh $d_{3z^2-r^2}$ states appearing in the lower energy region (−6.0 to −5.0 eV) below Fermi level. The corresponding partial charge density for the O−Rh interaction

is also presented for the Rh$_1$/MgO interface in panel (a) for comparison. We also find a strong Rh−Rh interaction in a relatively high energy region in the Rh$_n$/MgO systems with $n \geq$ 2. In the case of $n = 2$, the Rh dimer obtains electrons from the MgO surface, leading to a charge accumulation on the 4d orbitals. The Rh−Rh bonding states via the $d_{x^2-y^2}$ and d_{xy} interactions are clearly evident in the energy window (−3, −1.5) eV, as shown by the partial charge density. An antibonding e_g state associated with the Rh−Rh hybridization (a very localized state at an energy of −1.0 eV) is occupied by electrons, which can easily escape. For Rh$_3$, Rh$_4$, and Rh$_5$ on MgO, electrons obtained from the MgO surface are used nearly entirely for cluster binding.

2. Adsorption of a NO Molecule onto Rh$_n$/MgO (100) (n = 1−5). First, we calculated the adsorption energy of NO on free Rh$_n$ clusters, using the vdW-DF method on the basis of the stable NO binding geometries of Rh$_n$ clusters presented in ref 11. The most stable binding structures and adsorption energies of NO on each Rh$_n$ cluster are given in Table 3. The most

Table 3. Most Stable NO Binding Geometries on Rh_n Clusters, and the Corresponding Adsorption Energies[a]

Rh_n	1	2	3	4	5
Geometries					
E_{ads} (eV)	-3.97	-3.58	-3.37	-2.79	-2.80

[a]The N and O atoms are represented by violet and red spheres. The same color convention has been followed in Figure 6.

favored adsorption sites for NO on Rh_n clusters are consistent with the sites discussed in ref 11. The NO−Rh_1 complex has two degenerate configurations, a bent configuration and a straight line, with a N−O bond length of 1.18 Å. On a Rh dimer, NO tends to reside at the vertical bridge site, and the N−O bond length increases to 1.21 Å. On the Rh trimer, the configuration with the NO molecule positioned perpendicularly on the hollow site of the equilateral triangle is the configuration with the lowest total energy. The N−O bond length is about 1.23 Å. A tetrahedral Rh_4 cluster with an adsorbed NO has the lowest energy when the NO is somewhat askew at the bridge site between the two Rh atoms. This geometry was determined after optimization beginning from an initial state with the N atom occupying the hollow site on one of the triangular faces of tetrahedral Rh_4. For Rh_5, we considered only the ground state, that is, the square pyramid. In this case, it is most favorable for NO to bind in a bent configuration at the bridge site between two Rh atoms in the square face of Rh_5. The bond lengths of NO are 1.22 Å on both Rh_4 and Rh_5 clusters.

Clearly, NO has strong binding to small Rh_n clusters. The adsorption energies corresponding to the most stable configurations, as one proceeds from $n = 1$ to 5, are −3.97, −3.58, −3.37, −2.79, and −2.80 eV, respectively. It seems that the binding of NO gradually decreases as a function of cluster size. In the light of Bader charge analysis, as shown in Figure 5, Rh provides 0.35, 0.30, 0.22, 0.15, and 0.11 e to NO in each of the NO−Rh_n complexes, respectively. In addition, the loss of electrons induces a change in the spin state of the Rh_n clusters, but not always in the same direction. The NO−(Rh_1, Rh_2, Rh_3, and Rh_5) complexes decrease their total spin with respect to that of the bare clusters. In the cases of NO−(Rh_1 and Rh_3),
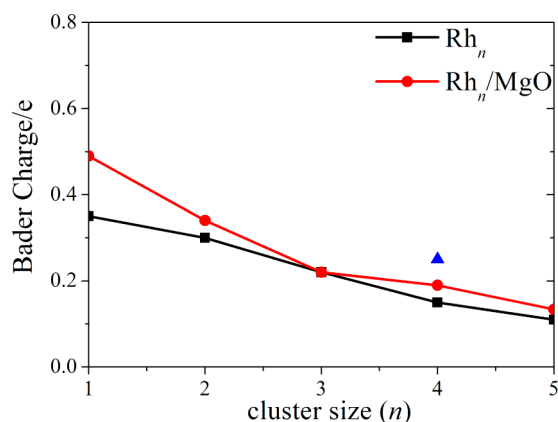

Figure 5. Average Bader charge (e) transferred from the Rh_n cluster to NO, with (red ●) and without (■) the MgO (100) surface, as a function of the cluster size (n). The blue "▲" shows the average charge provided from the square-Rh_4/MgO interface.

the complex is actually found to be nonmagnetic. With bonding to NO, the TMMs of Rh_2 and Rh_5 decrease by about 75% and 20%, respectively. However, the initially nonmagnetic tetrahedral Rh_4 exhibits strong spin polarization, with a TMM of 5.0 μ_B, when bonded to NO, correlating with the increase in the Rh−Rh bond length, which breaks the tetrahedral symmetry and induces the rearrangement of electrons in the 4d orbital. The trend of the total spin changes associated with NO adsorption in our work is consistent with that in ref 11, except in the case of tetrahedral Rh_4.

Next, we studied the adsorption of NO on Rh_n/MgO systems. The NO molecule was arranged to occupy different sites and to have various orientations as presented in ref 21, that is, horizontally on bridge and hollow sites (including the [100] and [110] directions), as well as vertically on the top, bridge, and hollow sites. We note that the initial position of the N or O atom was set to be slightly off the high symmetry site. Consequently, after full structural relaxation, NO can still bind near the hollow or bridge site, but its orientation is not necessarily exactly vertical or horizontal. We have calculated several stable configurations when NO binds to the Rh_n/MgO systems. The more stable structures are shown in Figure 6. The corresponding values of E_{ads} and d_{N-O} are also listed below each diagram.

In the Rh/MgO system, the Rh atom can strongly adsorb a tilted NO with an adsorption energy of −4.530 eV. Apparently, with the substrate, the single Rh atom exhibits a stronger ability to attract NO than does an isolated Rh atom. The N−O distance is 1.18 Å, almost the same as on an isolated Rh atom in vacuum. For Rh_2/MgO, due to the relatively long Rh−Rh bond, the dimer is found to adsorb NO horizontally. This configuration is slightly more stable than that in panel (c) with the NO positioned vertically above the bridge site. That is, in the horizontal orientation, both the N and the O atoms can bind to a Rh atom, resulting in an increased N−O bond length of 1.26 Å. In such a case, NO has a very strong binding to Rh_2/MgO with an energy of −4.365 eV, which is much stronger than that on the bare Rh dimer. The NO molecule has two degenerate adsorption sites on Rh_3/MgO as presented in panels (d) and (e) with the energy difference between them being only 0.02 eV. Additionally, the difference in the adsorption energies of NO on the trimer with and without the MgO surface is only 0.25 eV. Hence, there is a smaller contribution from the substrate than in other cases. There are several possible adsorption modes for NO on Rh_4/MgO. We put NO on various sites of the three Rh_4/MgO systems shown in Figure 1f−h. For the two tetrahedral-Rh_4/MgO complexes, the NO molecule was initially placed on the vertical bridge sites and the vertical hollow site on one of the triangular faces. After optimization, the configuration with NO binding on the hollow site of one triangular face of the Rh_4 cluster with three Rh
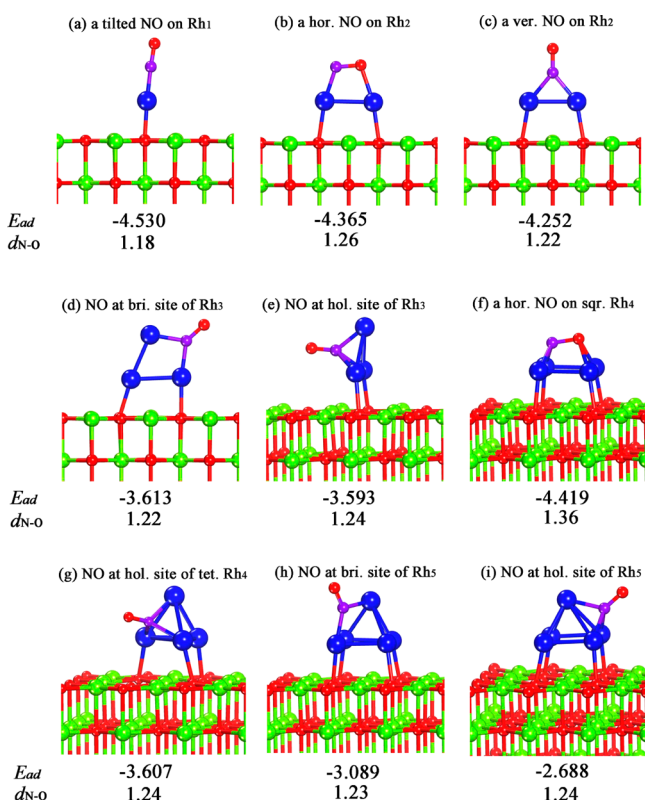
Figure 6. Energetically preferred NO adsorption structures on the Rh$_n$/MgO systems. (a) NO on a single Rh atom, (b and c) NO residing at the bridge site of Rh$_2$ with horizontal and vertical orientations, (d and e) NO at the bridge and hollow sites of Rh$_3$, (f) NO horizontally at the hollow site of a square Rh$_4$, (g) NO occupying the hollow site on one of the triangular faces of tetrahedral Rh$_4$, and (h and i) NO at the bridge and hollow sites of Rh$_5$. Below each diagram, the calculated E_{ads} (according to eq 2, in eV) and d_{N-O} (in Å) for NO are also presented.

atoms bonded to the support (shown in Figure 6g) was found to be the most stable. In this case, NO has an adsorption energy of −3.607 eV. On the square-Rh$_4$/MgO system, we initially put NO on the top, vertical/horizontal bridge, and vertical/horizontal hollow sites. After full optimization, the most stable configuration with the lowest total energy was found to correspond to the complex with NO horizontally bonded on the hollow site of the Rh square (see Figure 6h). The N and O

atoms bind to two Rh atoms, leading to the length of the N−O bond undergoing a large increase to 1.36 Å. The adsorption energy of NO on the square Rh$_4$/MgO system is −4.419 eV, much lower than that on the bare Rh$_4$ cluster (−2.790 eV). Moreover, because the calculated total energy of the NO-square-Rh$_4$/MgO is 0.292 eV lower than that for NO-tetrahedral-Rh$_4$/MgO, the former is more stable than the latter. Thus, the adsorption of NO improves the stability of square-Rh$_4$/MgO. Although the configuration in panel (g) is less stable than the former one (panel (f)), it still improves the binding of NO to tetrahedral Rh$_4$/MgO. Finally, for NO bonded to one of the apex edges of the square pyramid Rh$_5$, panel (i), NO is in a somewhat tilted position and has an adsorption energy of −3.089 eV. The length of the N−O bond is about 1.23 Å, consistent with that in the NO−Rh$_5$ complex. Similar to the case of NO on Rh$_3$/MgO, the improvement of Rh$_5$/MgO for trapping NO as compared to bare Rh$_5$ is very limited.

To explore the interactions between NO and the Rh$_n$ or Rh$_n$/MgO (100) systems, we have calculated the three-dimensional charge density differences and show them in Figure 7. The values were calculated using

$$\Delta\rho = \rho(\text{NO/substrate}) - \rho(\text{NO}) - \rho(\text{substrate})$$

in which $\rho(\text{NO/substrate})$ is the total charge density of the system with NO binding on either Rh$_n$ or Rh$_n$/MgO (100), $\rho(\text{NO})$ is the charge density of the free NO molecule in its adsorbed geometry, and $\rho(\text{substrate})$ represents the charge density of the substrate (Rh$_n$ or Rh$_n$/MgO) all for the relaxed geometry after adsorption. Comparing with the NO−Rh$_n$ complexes, it may be seen that more electrons are found to accumulate on the Rh−N and Rh−O bonds of the NO−Rh$_n$/MgO complex than on the corresponding bonds for isolated Rh$_n$ clusters. This is especially true for the cases shown in panels (a), (b), and (d) of Figure 7. We can also obtain the same result from Figure 5 (the Bader charge analysis), that the Rh$_n$/MgO (n = 1, 2, and 4) systems transfer more electrons to NO than do the bare Rh$_n$ clusters. For NO adsorption on Rh/MgO, we can see a greater accumulation of electrons between the N and Rh atoms. Figure 5 also shows that NO obtains 0.49 e and 0.35 e from Rh/MgO and Rh, respectively. Thus, NO has a rather stronger binding to Rh/MgO than it has to a single Rh atom. In the case of n = 2, there are two distinct adsorption modes for NO on Rh$_2$ and Rh$_2$/MgO. On a Rh dimer, NO resides vertically above the dimer, and we find charge
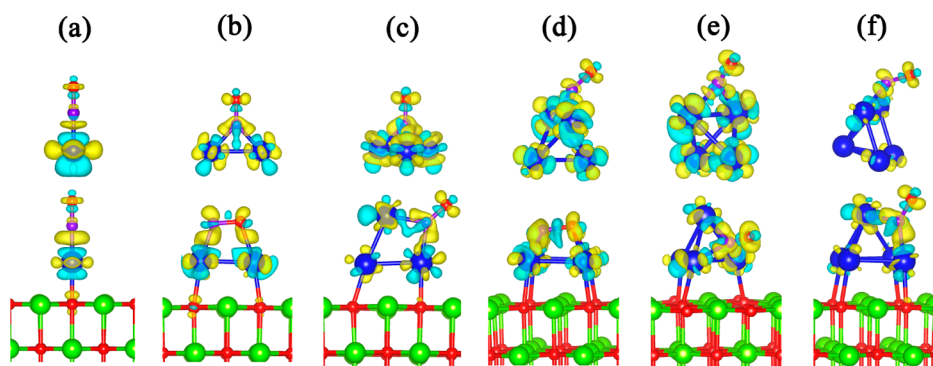

Figure 7. Panels (a)−(f) show charge density differences for the system with Rh$_n$ (n = 1−5) adsorbing NO, with and without the MgO (100) surface. Panels (d) and (e) are for the square and tetrahedral Rh$_4$ clusters, respectively. The yellow and blue regions indicate charge accumulation and depletion, respectively. The isosurface value is 0.01 e/Å^3.
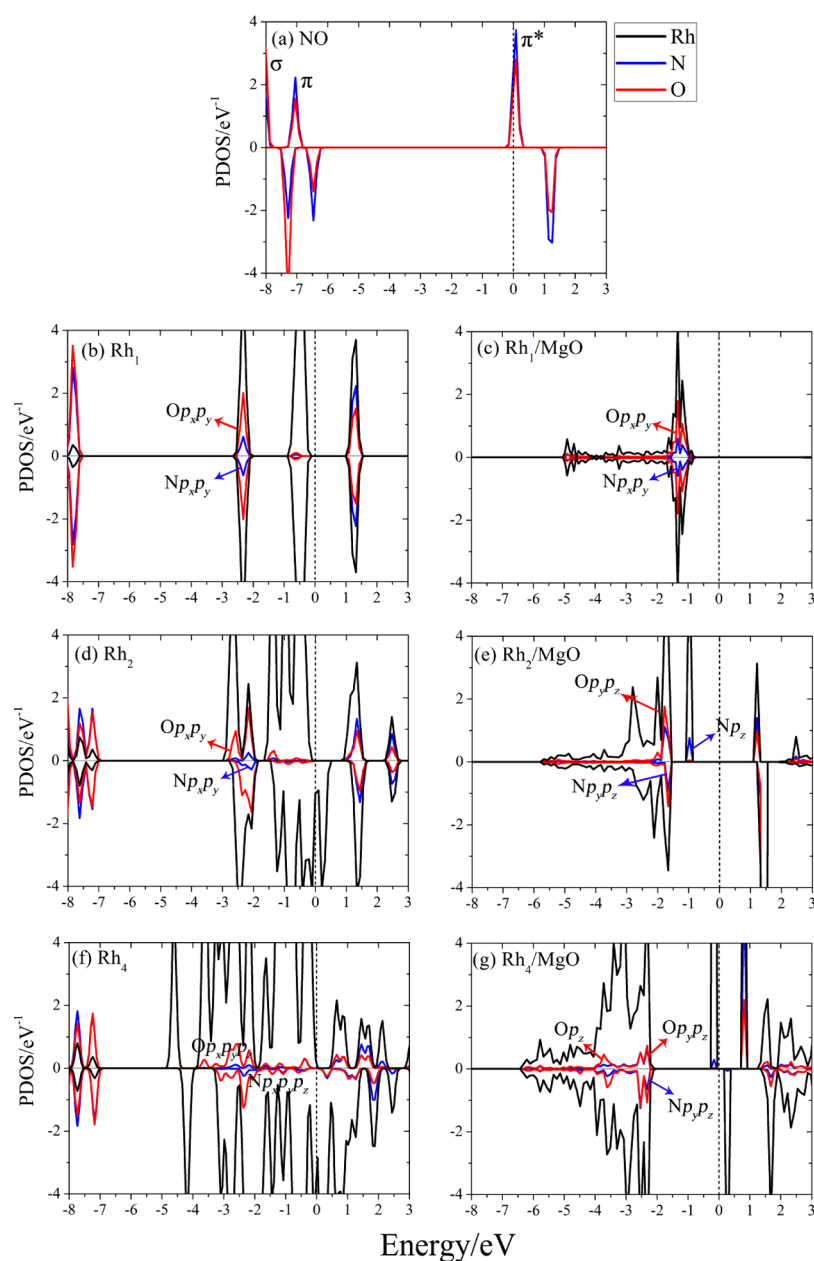
Figure 8. Calculated PDOS for the systems with NO binding on (b) single Rh, (c) Rh_1/MgO, (d) Rh dimer, (e) Rh_2/MgO, (f) Rh_4, and (g) square Rh_4/MgO. To ease comparison, the DOS for the NO molecule is plotted in (a). The black, blue, and red lines represent the total DOS of the Rh_n (n = 1, 2, and 4-square), N, and O atoms, respectively. The Fermi level is set to zero.

accumulation on the two Rh−N bonds and depletion between the two Rh atoms. The dimer donates 0.61 e to NO in all. When the dimer is deposited on the MgO (100) surface, the N and O atoms align horizontally on the Rh dimer. The accumulation of electrons on the Rh−N and Rh−O bonds indicates that both N and O can bind strongly to Rh atoms, but this results in a slightly weakened N−O bond shown by the tiny depletion region between them. Similarly, the N and O atoms are also found to align horizontally on the square-Rh_4/MgO interface. The bottom panel of Figure 7d shows that a significant amount of charge transfers from the Rh atoms to NO, indicating the strong interaction of the Rh−N and Rh−O bonds. The notable charge depletion between N and O means that the NO molecular bond is dramatically weakened as the N and O atoms withdraw extra charge from the square Rh_4/MgO interface. Although the tetrahedral-Rh_4/MgO interface is not as

good as the square one for trapping the NO molecule, it is still more favorable than the bare tetrahedral-Rh_4 cluster. The NO molecule obtains 0.61, 0.77, and 1.01 e from the tetrahedral-Rh_4 cluster and the tetrahedral- and square-Rh_4/MgO systems, respectively. From Figure 7c and f, we find that the charge accumulation at the Rh−N bonds in the presence of the MgO substrate looks slightly stronger than that for bare clusters. Bader charge analysis shows that with the MgO substrate, Rh_3 (Rh_5) provides 0.68 e (0.63 e) to NO, 0.03 e (0.07 e) more than do the bare Rh_3 (Rh_5) clusters. As a result, with a MgO (100) surface substrate, N/O can tightly bind to Rh_n through obtaining more electrons from the combined Rh_n/MgO system, especially for Rh_1, Rh_2, and square-Rh_4/MgO interfaces. This is why the Rh_n/MgO interfaces exhibit improved capacity for trapping NO as compared to bare Rh_n clusters.
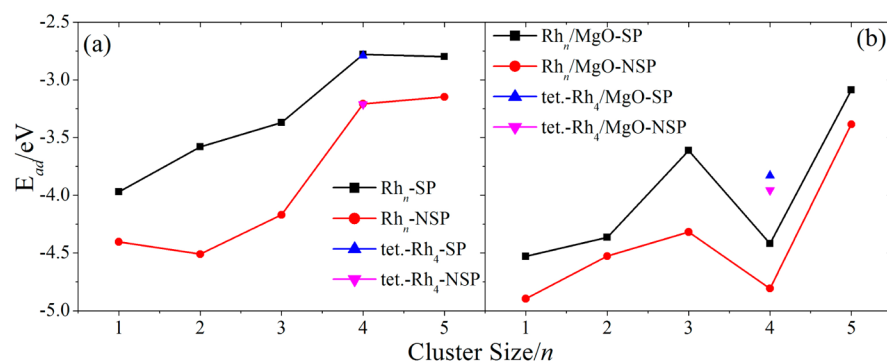
Figure 9. Adsorption energies, E_{ads}, of NO on (a) Rh_n clusters and (b) Rh_n/MgO as a function of the cluster size (n). The "■" denote the spin-polarized (SP) results, whereas the red "●" denote the nonspin-polarized (NSP) results. The blue "▲" and magenta "▼" denote the E_{ads} of NO on tetrahedral-Rh_4 with and without the MgO surface in the SP and NSP cases, respectively.

With a MgO (100) surface as substrate, the binding of NO to Rh_1, Rh_2, and square-Rh_4 clusters is significantly improved. To better perceive the differences between the NO−Rh_n interaction (n = 1, 2, and 4) for the cases of the isolated clusters and the clusters on a MgO surface, we have used PDOS analysis (Figure 8). The NO states around −8.0 eV are derived from the σ and π molecular orbitals, while the states with higher energies are assigned to π^* states. In the case of NO binding on the isolated clusters, the Rh 4d and NO molecular-orbital hybridization appearing in the energy range of $[-3.0, 0.0]$ eV looks rather weak, as compared to the Rh−Rh interaction near the Fermi level and the N−O bonding state in the lower energy region. In contrast, in the presence of the substrate, the obvious hybridization between the Rh d and N/O p orbitals, as well as the strong interaction between Rh clusters and the substrate mentioned above, lead to a downward shift of the Rh−Rh bonding states to below the Fermi level. For a single Rh atom, due to the interaction between Rh and NO (the NO bond is along the z axis), the π^* states (π_x^* and π_y^*) obtain electrons from Rh, leading to a downward shift beneath the Fermi level. The Rh 4d and NO π^* states remain localized. When a Rh atom is deposited on a MgO surface, the extensive hybridization between Rh 4d and NO molecular orbitals induces a broadening of the NO π^* (π_x^* and π_y^*) state. On a Rh dimer and tetrahedron, NO (along the z axis) binds to the Rh atoms through hybridization of the Rh 4d and N p orbitals. For the NO−Rh_2/MgO system, the NO bond is along the x axis. The strong Rh−NO interaction derives from the hybridization between Rh 4d and the combined effect of the NO π_z^* and π_y^* states. A similar result can also be found in the case of the NO−Rh_4/MgO system where the NO molecule binds horizontally to Rh_4/MgO. The significant NO−Rh interaction is due to the hybridizations of the Rh 4d-N $2p_y$ and Rh 4d-O $2p_z$ and $2p_y$ states. In addition, the bonding states of the NO molecule vanish even in the much lower energy region. As a result, the interaction of NO with the Rh_n cluster deposited on the MgO (100) surface is much stronger than that with the bare Rh_n clusters, and the molecular bond of NO is thereby greatly weakened.

The TMMs of Rh_n in the NO−Rh_n/MgO systems are listed in Table 2. In all cases, the NO adsorption suppresses the magnetism of Rh_n. As expected, the Rh atoms that are directly bonded to NO are found to lose magnetism most strongly, while the others remain essentially unchanged. Moreover, the reduced amplitudes of TMMs induced by NO adsorption on Rh_n/MgO are smaller than those for the bare Rh_n clusters,

except in the case of square-Rh_4/MgO. To clarify whether the enhanced interaction between NO and Rh_n/MgO can be related to the reduction in the magnitude of the TMMs of Rh_n, one has to know the adsorption energies of NO on Rh_n and Rh_n/MgO without spin-polarization, and compare the values with those obtained in spin-polarized (SP) calculations.

We have therefore redone the calculations for NO adsorption on Rh_n clusters with and without the substrate for the nonspin polarized (NSP) case. All of the results are available in Figure 9. It may be seen that when the Rh_n clusters are constrained to be nonmagnetic, there is a noticeable impact on the NO adsorption energy, independent of the MgO surface substrate. It may be seen that our NSP calculations yielded lower values for the NO adsorption energies than were obtained with the SP calculations. In addition, with the MgO surface, the adsorption energy differences between the SP and NSP cases seem smaller than those obtained for the NO−Rh_n systems. The most prominent differences are for the NO−Rh_2/MgO and NO−tetrahedral-Rh_4/MgO systems. Here, the differences appear to be consistent with the differences in the TMM changes in the Rh_n clusters associated with NO adsorption on Rh_n and Rh_n/MgO, as shown in Table 2. However, square-Rh_4/MgO is an exceptional case. Generally, the greatly suppressed TMM would be expected to correspond to a large decrease of binding of Rh_n clusters to NO, due to the competition between bonding and magnetism discussed by Ghosh et al. in ref 11. From Table 2, it may be seen that the reduction in the TMM of the square-Rh_4/MgO system (4.78 μ_B) is greater than that for the square-Rh_4 cluster (1.0 μ_B), with NO adsorption. However, the large TMM reduction does not have any remarkable impact on the NO bonding. For the square-Rh_4, for either the bare cluster or the cluster deposited on an MgO surface, the difference in the NO adsorption energy between the SP and NSP cases is about 0.4 eV, as shown in Figure 9. We feel that the significantly enhanced binding of NO to square-Rh_4/MgO is due to the change in the NO adsorption mode; that is, all of the Rh atoms are involved in bonding to the N and O atoms, which align horizontally above the Rh_4 square. In addition, the fact that the square-Rh_4/MgO interface donates more electrons to NO results in it losing essentially all of its TMM. The same conclusion can be obtained from the PDOS analysis in Figure 8g as well. As a result, changes in the TMM of the Rh_n clusters on the MgO surface are insufficient to account for the improved binding effect to NO. Although depositing on a MgO surface reduces the effective coordination number of the Rh_n clusters, the competition between the bonding and the effects

of the changes in magnetism is ambiguous and deserves further investigation.

IV. SUMMARY

We have performed spin-polarized first-principles calculations to investigate the interactions and morphologies of small Rh_n clusters ($n \leq 5$) deposited on the MgO (100) surface, as well as the ability of the Rh_n/MgO systems to trap NO molecules. The MgO (100) surface can strongly adsorb Rh_n clusters through the hybridization of the O 2p and Rh 4d orbitals. When Rh_n clusters interact with the MgO surface, their most energetically preferred structures are similar to those of the isolated clusters, except for an increment in the lengths of the Rh−Rh bonds in the base edge(s) close to the substrate. The interfacial interaction of Rh_n/MgO not only increases the lengths of Rh−Rh bonds, but also causes the Rh atoms to obtain extra electrons from the substrate. The result is that the Rh_n/MgO systems exhibit a much stronger ability to trap NO than do bare Rh_n clusters, especially in the cases of Rh_1, Rh_2, and Rh_4. When Rh_n/MgO adsorbs NO, the NO molecule obtains additional electrons from the Rh_n clusters, indicating stronger binding for N/O−Rh bonds, and, in turn, dramatic weakening of the N−O molecular interaction. With a MgO (100) surface as substrate, the competition between magnetism and bonding effects is less significant than for isolated clusters, despite the reduced effective coordination number. However, this reduced competition is not sufficient to explain the improved ability of the Rh_n/MgO systems to trap NO molecules. Thus, we have proposed that putting Rh_n clusters on MgO can significantly improve the catalytic activity of Rh_n clusters for NO dissociation. We also plan to investigate the NO−Rh_n interactions on other metal−oxide surfaces.

■ AUTHOR INFORMATION

Corresponding Author
*Tel.: 86-0311-80787350. E-mail: zxtian@mail.hebtu.edu.cn.
Notes
The authors declare no competing financial interest.

■ ACKNOWLEDGMENTS

■ REFERENCES

(1) Loffreda, D.; Simon, D.; Sautet, P. Molecular and Dissociative Chemisorption of NO on Palladium and Rhodium (100) and (111) Surfaces: A Density-Functional Periodic Study. *J. Chem. Phys.* **1998**, *108*, 6447.

(2) Beyer, M. K.; Knickelbein, M. B. Electric Deflection Studies of Rhodium Clusters. *J. Chem. Phys.* **2007**, *126*, 104301.

(3) Cox, A. J.; Louderback, J. G.; Apsel, S. E.; Bloomfield, L. A. Magnetism in 4d-Transition Metal Clusters. *Phys. Rev. B: Condens. Matter Mater. Phys.* **1994**, *49*, 12295.

(4) Nieuwenhuys, B. E. The Surface Science Approach Toward Understanding Automotive Exhaust Conversion Catalysis at the Atomic Level. *Adv. Catal.* **1999**, *44*, 259−328.

(5) Balteanu, I.; Achatz, U.; Balaj, O. P.; Fox, B. S.; Beyer, M.; Bondybey, V. E. The Effect of Charge upon CO-Adsorption by Ionic Group 5 and Group 9 Transition Metal Clusters. *Int. J. Mass Spectrom.* **2003**, *229*, 61−65.

(6) Ford, M. S.; Anderson, M. L.; Barrow, M. P.; Woodruff, D. P.; Drewello, T.; Derrick, P. J.; Mackenzie, S. R. Reactions of Nitric Oxide on Rh^{6+} Clusters: Abundant Chemistry and Evidence of Structural Isomers. *Phys. Chem. Chem. Phys.* **2005**, *7*, 975−980.

(7) Anderson, M. L.; Ford, M. S.; Derrick, P. J.; Drewello, T.; Woodruff, D. P.; Mackenzie, S. R. Nitric Oxide Decomposition on Small Rhodium Clusters, $Rh_n^{\pm}$. *J. Phys. Chem. A* **2006**, *110*, 10992−11000.

(8) Harding, D.; Ford, M. S.; Walsh, T. R.; Mackenzie, S. R. Dramatic Size Effects and Evidence of Structural Isomers in the Reactions of Rhodium Clusters, $Rh_n^{\pm}$, with Nitrous Oxide. *Phys. Chem. Chem. Phys.* **2007**, *9*, 2130−2136.

(9) Pan, X.; Fan, Z.; Chen, W.; Ding, Y.; Luo, H.; Bao, X. Enhanced Ethanol Production inside Carbon-Nanotube Reactors Containing Catalytic Particles. *Nat. Mater.* **2007**, *6*, 507−511.

(10) Harding, D. J.; Davies, R. D. L.; Mackenzie, S. R.; Walsh, T. R. Oxides of Small Rhodium Clusters: Theoretical Investigation of Experimental Reactivities. *J. Chem. Phys.* **2008**, *129*, 124304.

(11) Ghosh, P.; Pushpa, R.; de Gironcoli, S.; Narasimhan, S. Interplay between Bonding and Magnetism in the Binding of NO to Rh Clusters. *J. Chem. Phys.* **2008**, *128*, 194708.

(12) Pushpa, R.; Ghosh, P.; de Gironcoli, S.; Narasimhan, S. Effective Coordination Number: A Simple Indicator of Activation Energies for NO dissociation on Rh(100) Surfaces. *Phys. Rev. B: Condens. Matter Mater. Phys.* **2009**, *80*, 233406.

(13) Reddy, B. V.; Khanna, S. N.; Dunlap, B. I. Giant Magnetic Moments in 4d Clusters. *Phys. Rev. Lett.* **1993**, *70*, 3323.

(14) Cox, A. J.; Louderback, J. G.; Bloomfield, L. A. Experimental Observation of Magnetism in Rhodium Clusters. *Phys. Rev. Lett.* **1993**, *71*, 923.

(15) Bae, Y.-C.; Osanai, H.; Kumar, V.; Kawazoe, Y. Nonicosahedral Growth and Magnetic Behavior of Rhodium Clusters. *Phys. Rev. B: Condens. Matter Mater. Phys.* **2004**, *70*, 195413.

(16) Harding, D.; Mackenzie, S. R.; Walsh, T. R. Structural Isomers and Reactivity for Rh_6 and Rh_6^+. *J. Phys. Chem. B* **2006**, *110*, 18272.

(17) Bertin, V.; Lopez-Rendón, R.; del Angel, G.; Poulain, E.; Avilés, R.; Uc-Rosas, V. Comparative Theoretical Study of Small Rh_n Nanoparticles ($2 \leq n \leq 8$) using DFT Methods. *Int. J. Quantum Chem.* **2010**, *110*, 1152−1164.

(18) Da Silva, J. L. F.; Piotrowski, M. J.; Aguilera-Granja, F. Hybrid Density Functional Study of Small Rh_n (n = 2−15) Cluster. *Phys. Rev. B: Condens. Matter Mater. Phys.* **2012**, *86*, 125430.

(19) Endou, A.; Yamauchi, R.; Kubo, M.; Stirling, A.; Miyamoto, A. Adsorption of NO on Rhodium and Palladium Clusters: A Density Functional Study. *Appl. Surf. Sci.* **1997**, *119*, 318−320.

(20) Torres, M. B.; Aguilera-Granja, F.; Balbás, L. C.; Vega, A. Ab Initio Study of the Adsorption of NO on the Rh_6^+ Cluster. *J. Phys. Chem. A* **2011**, *115*, 8350−8360.

(21) Pushpa, R.; Ghosh, P.; Narasimhan, S.; de Gironcoli, S. Effective Coordination as a Predictor of Adsorption Energies: A Model Study of NO on Rh(100) and Rh/MgO(100) Surfaces. *Phys. Rev. B: Condens. Matter Mater. Phys.* **2009**, *79*, 165406.

(22) Yang, W.; Wang, Z.; Wang, Z.; Yang, Z.; Xia, C.; Peng, R.; Wu, X.; Lu, Y. Enhanced Catalytic Activity toward O_2 Reduction on Pt-Modified $La_{1−x}Sr_xCo_{1−y}Fe_yO_{3−\delta}$ Cathode: A Combination Study of First-Principles Calculation and Experiment. *ACS Appl. Mater. Interfaces* **2014**, *6*, 21051−21059.

(23) Chen, J. J.; Wang, W. K.; Li, W. W.; Pei, D. N.; Yu, H. Q. Roles of Crystal Surface in Pt-Loaded Titania for Photocatalytic Conversion of Organic Pollutants: A First-Principle Theoretical Calculation. *ACS Appl. Mater. Interfaces* **2015**, *7*, 12671−12678.

(24) Dong, Y. F.; Wang, S. J.; Mi, Y. Y.; Feng, Y. P.; Huan, A. C. H. First-Principles Studies on Initial Growth of Ni on MgO(0 0 1) Surface. *Surf. Sci.* **2006**, *600*, 2154−2162.

(25) Gao, D. Z.; Watkins, M. B.; Shluger, A. L. Transient Mobility Mechanisms of Deposited Metal Atoms on Insulating Surfaces: Pd on MgO (100). *J. Phys. Chem. C* **2012**, *116*, 14471−14479.

(26) Yang, Z.; Wu, R.; Zhang, Q.; Goodman, D. W. Adsorption of Au on an O-Deficient MgO(001) Surface. *Phys. Rev. B: Condens. Matter Mater. Phys.* **2002**, *65*, 155407.

(27) He, B.; Ma, D.; Hao, W.; Xiao, W.; Tian, Z. Ag (100)/MgO (100) Interface: A van der Waal Density Functional Study. *Appl. Surf. Sci.* **2014**, *288*, 115−121.

(28) Kresse, G.; Hafner, J. Ab initio Molecular Dynamics for Liquid Metals. *Phys. Rev. B: Condens. Matter Mater. Phys.* **1993**, *47*, 558.

(29) Kresse, G.; Furthmüller, J. Efficiency of Ab Initio Total Energy Calculations for Metals and Semiconductors Using a Plane-Wave Basis Set. *Comput. Mater. Sci.* **1996**, *6*, 15−50.

(30) Kresse, G.; Furthmüller, J. Efficient Iterative Schemes for Ab Initio Total-Energy Calculations Using a Plane-Wave Basis Set. *Phys. Rev. B: Condens. Matter Mater. Phys.* **1996**, *54*, 11169.

(31) Blöchl, P. E. Projector Augmented-Wave Method. *Phys. Rev. B: Condens. Matter Mater. Phys.* **1994**, *50*, 17953.

(32) Kresse, G.; Joubert, D. From Ultrasoft Pseudopotentials to the Projector Augmented-Wave Method. *Phys. Rev. B: Condens. Matter Mater. Phys.* **1999**, *59*, 1758.

(33) Perdew, J. P.; Zunger, A. Self-Interaction Correction To Density-Functional Approximations For Many-Electron Systems. *Phys. Rev. B: Condens. Matter Mater. Phys.* **1981**, *23*, 5048−5079.

(34) Perdew, J. P.; Burke, K.; Ernzerhof, M. Generalized Gradient Approximation Made Simple. *Phys. Rev. Lett.* **1996**, *77*, 3865.

(35) Dion, M.; Rydberg, H.; Schröder, E.; Langreth, D. C.; Lundqvist, B. I. Van der Waals Density Functional for General Geometries. *Phys. Rev. Lett.* **2004**, *92*, 246401.

(36) Klimeš, J.; Bowler, D. R.; Michaelides, A. Van der Waals Density Functionals Applied to Solids. *Phys. Rev. B: Condens. Matter Mater. Phys.* **2011**, *83*, 195131.

(37) Román-Pérez, G.; Soler, J. M. Efficient Implementation of a Van der Waals Density Functional: Application to Double-Wall Carbon Nanotubes. *Phys. Rev. Lett.* **2009**, *103*, 096102.

(38) Monkhorst, H. J.; Pack, J. D. Special Points for Brillouin-Zone Integrations. *Phys. Rev. B* **1976**, *13*, 5188.

(39) Shi, X. R.; Sholl, D. S. Nucleation of Rh_n (n = 1−5) Clusters on γ-Al_2O_3 Surfaces: A Density Functional Theory Study. *J. Phys. Chem. C* **2012**, *116*, 10623−10631.

(40) Nayak, S. K.; Weber, S. E.; Jena, P.; Wildberger, K.; Zeller, R.; Dederichs, P. H.; Stepanyuk, V. S.; Hergert, W. Relationship Between Magnetism, Topology, and Reactivity of Rh Clusters. *Phys. Rev. B: Condens. Matter Mater. Phys.* **1997**, *56*, 8849−8854.

(41) Gingerich, K. A.; Cocke, D. L. Thermodynamic Confirmation for the High Stability of Gaseous TiRh as Predicted by the Brewer-Engel Metallic Theory and the Dissociation Energy of Diatomic Rhodium. *J. Chem. Soc., Chem. Commun.* **1972**, *9*, 536.

(42) Reddy, B. V.; Nayak, S. K.; Khanna, S. N.; Rao, B. K.; Jena, P. Electronic Structure and Magnetism of Rh_n (n = 2−13) clusters. *Phys. Rev. B: Condens. Matter Mater. Phys.* **1999**, *59*, 5214−5222.

(43) Chien, C.-H.; Blaisten-Barojas, E.; Pederson, M. R. Magnetic and Electronic Properties of Rhodium Clusters. *Phys. Rev. A: At., Mol., Opt. Phys.* **1998**, *58*, 2196−2202.

(44) Delley, B. An All-Electron Numerical Method for Solving the Local Density Functional for Polyatomic Molecules. *J. Chem. Phys.* **1990**, *92*, 508−517.

(45) Giannozzi, P.; Baroni, S.; Bonini, N.; Calandra, M.; Car, R.; Cavazzoni, C.; Ceresoli, D.; Chiarotti, G. L.; Cococcioni, M.; Dabo, I.; Corso, A. D.; Gironcoli, S. D.; Fabris, S.; Fratesi, G.; Gebauer, R.; Gerstmann, U.; Gougoussis, C.; Kokali, A.; Lazzeri, M.; Martin-Samos, L.; Marzari, N.; Mauri, F.; Mazzarello, R.; Paolini, S.; Pasquarello, A.; Paulatto, L.; Sbraccia, C.; Scandolo, S.; Sclauzero, G.; Seitsonen, A. P.; Smogunov, A.; Umari, P.; Wentzcovitch, R. M. QUANTUM ESPRESSO: A Modular and Open-Source Software Project for Quantum Simulations of Materials. *J. Phys.: Condens. Matter* **2009**, *21*, 395502.

(46) Chen, Y.; Huo, M.; Chen, T.; Li, Q.; Sun, Z.; Song, L. The Properties of Ir_n (n = 2−10) Clusters and Their Nucleation on γ-Al_2O_3 and MgO Surfaces: From *Ab Initio* studies. *Phys. Chem. Chem. Phys.* **2015**, *17*, 1680−1687.